Journal of Alloys and Compounds 842 (2020) 155763

Contents lists available at ScienceDirect

Journal of Alloys and Compounds

journal homepage: http://www.elsevier.com/locate/jalcom

Thermodynamic and resonant properties of mixed spin compounds $ACuFe_2(VO_4)_3$ (A = Li, Na)

A. Koshelev [a, b], L. Shvanskaya [a, c], O. Volkova [a, m], K. Zakharov [a], F. Theuss [d], C. Koo [d], R. Klingeler [d, e], S. Kamusella [f], H.-H. Klauss [f], S. Kundu [g, h], S. Bachhar [g], A.V. Mahajan [g], P. Khuntia [h], D. Khanam [i], B. Rahaman [i], T. Saha-Dasgupta [j, k], A. Vasiliev [a, l, m, *]

[a] Lomonosov Moscow State University, 119991, Moscow, Russia
[b] Institute of Experimental Mineralogy, RAS, 142432, Chernogolovka, Russia
[c] National University of Science and Technology "MISiS", 119049, Moscow, Russia
[d] Kirchhoff Institute for Physics, Heidelberg University, 69120, Heidelberg, Germany
[e] Centre for Advanced Materials, Heidelberg University, 69120, Heidelberg, Germany
[f] Technical University Dresden, 01069, Dresden, Germany
[g] Department of Physics, Indian Institute of Technology Bombay, 400076, Mumbai, India
[h] Department of Physics, Indian Institute of Technology Madras, 600036, Chennai, India
[i] Aliah University, 700156, Kolkata, India
[j] S.N. Bose Natl Ctr Basic Sci, 700098, Kolkata, India
[k] Indian Assoc Cultivat Sci, 700032, Kolkata, India
[l] National Research South Ural State University, 454080, Chelyabinsk, Russia
[m] Ural Federal University, 620002, Ekaterinburg, Russia

ARTICLE INFO

Article history:
Received 16 April 2020
Received in revised form
20 May 2020
Accepted 21 May 2020
Available online 9 June 2020

Keywords:
Multiferroicity
Howardevansite
NMR
ESR
Moessbauer spectroscopy
First principles calculations

ABSTRACT

We report a combined experimental and theoretical study on magnetism and magneto-electric coupling in howardevansite-type mixed-spin chain compounds $ACuFe_2(VO_4)_3$ (A = Li, Na). While $LiCuFe_2(VO_4)_3$ shows long-range magnetic order and spin-order-induced ferroelectricity, i.e., multiferroicity of type II, neither magnetic order nor magneto-electric effects are observed in the Na-based sister compound. Notably, our local magnetic probes studies by means of NMR, ESR, and Mössbauer spectroscopy evidence similar magnetic behavior of both compounds at the time scales of these experiments. This is confirmed by first principles calculations which imply a similar hierarchy of exchange interaction parameters. Our results suggest that the absence of magneto-electric effects in $NaCuFe_2(VO_4)_3$ as seen in bulk measurements is a disorder effect associated with lower mobility of Na ions within the channels of the crystal structure as compared to the mobility of Li ions, thereby presenting a yet disregarded degree of freedom to tune the multiferroicity.

1. Introduction

Materials which experience more than one of the basic ferroic properties are named multiferroics. Following Daniel Khomskii [1], these materials can be classified into type I and type II categories. Type II multiferroics, where magnetic order breaks inversion symmetry and causes ferroelectricity, are rare and fragile [2]. It has been shown recently, that the mixed spin chain compound $LiCuFe_2(VO_4)_3$ belongs to this class, exhibiting a magneto-electric effect in the temperature range between $T_{N1} = 8.2$ K and $T_{N2} = 9.8$ K, both temperatures being associated with ordering and reordering of the magnetic subsystem [3]. Both transitions are marked by sharp singularities in dielectric permittivity ε which are preceded by a relaxation-type anomaly at about 30 K similar to that observed in Li_2CuZrO_4 where the Li ions freeze statistically in the half-filled position [4]. Similarly, coupling of a glass-like alkali metal subsystem to the magnetic one may influence quantum critical behavior of the system. To check this assumption we have synthesized and performed a comprehensive study of thermodynamic and resonant properties of howardevansite-type compounds, $ACuFe_2(VO_4)_3$ (A = Li, Na), accompanied by first principles calculations of exchange interaction parameters.

* Corresponding author. Lomonosov Moscow State University, 119991, Moscow, Russia.
E-mail address: vasil@mig.phys.msu.ru (A. Vasiliev).

https://doi.org/10.1016/j.jallcom.2020.155763
0925-8388/

$NaCuFe_2(VO_4)_3$ is a mineral, howardevansite, whose crystal structure belongs to the symmetry group $P\bar{1}$ [5]. It contains serpentine chains of edge-sharing CuO_5 pyramids and pairs of FeO_6 octahedra. The chains are linked to each other through VO_4 tetrahedra forming a three-dimensional framework structure. The channels of the structure are filled with Na ions in two distinctly different positions, one of which is half-filled. The lithium compound, $LiCuFe_2(VO_4)_3$, is isostructural with its sodium counterpart [6].

The fact that one of the alkali ions position within the [001] channels is occupied statistically implies randomness in the spatial distribution of the positive charge in the lattice. Typically, this randomness is affected by temperature since alkali ions may be mobile at sufficiently high temperatures but tend to freeze upon cooling. This is reflected by conductivity of $LiCuFe_2(VO_4)_3$ and $NaCuFe_2(VO_4)_3$ which have been studied recently [7,8]. It has been shown that the electrical conductivity is governed by hopping of alkali ions within the channels, but the details of this hopping differ significantly. In $LiCuFe_2(VO_4)_3$, the mechanism of ionic conductivity is a correlated barrier hopping mechanism with activation energy $E_a = 0.66$ eV and effective attempt frequency $\omega_0 = 1.48 \times 10^{12} s^{-1}$ [7], while in $NaCuFe_2(VO_4)_3$ $E_a = 0.87$ eV and $\omega_0 = 1.28 \times 10^{13} s^{-1}$ but the hopping is associated with single ion motion [8].

2. Experimental details

Powder samples of $ACuFe_2(VO_4)_3$ were obtained via solid-state reaction of Li_2CO_3 or Na_2CO_3, Fe_2O_3, CuO and V_2O_5. They were taken in stoichiometric ratio, calcinated and annealed in air at 600 and 640 °C for 72 h with intermediate grinding. Phase purity of the samples was confirmed by powder X-Ray Diffraction using an ADP Diffractometer (Co K_α radiation, $\lambda = 1.789010$ Å).

The specific heat capacity C_p as well as the *ac* and *dc* magnetic susceptibility χ of $ACuFe_2(VO_4)_3$ in the range 2–300 K were measured using the Quantum Design PPMS – 9T. The dielectric permittivity ε was measured in the frequency range $f = 10 \div 10^3$ Hz by means of Andeen-Hagerling 2700A capacitance bridge.

NMR measurements were carried out using a phase-coherent Tecmag spectrometer in the range 4–300 K at applied field $B = 9.3954$ T. Fixed field NMR absorption spectra, spin-lattice relaxation rate ($1/T_1$) and spin-spin relaxation rate ($1/T_2$) were measured using a conventional spin-echo sequence ($\pi/2$-τ_{echo}-π). The standard spin-echo pulse sequence with a variable delay time τ_D was used to measure T_2 and a saturation pulse sequence ($\pi/2$-τ_D-π) was used to measure T_1. A comb of saturating *rf* pulses for T_1 measurements was employed to obtain better longitudinal nuclear magnetization.

Electron Spin Resonance (ESR) studies were carried out in a Bruker Elexsys E500 X-band spectrometer on a powder sample. The setup uses a high sensitivity ER 4122 SHQE continuous wave resonator and operates at frequencies around 9.63 GHz and in magnetic fields up to 1.2 T. Temperature variation between 4 K and 300 K has been realized in a cryo-free setup.

3. Bulk properties

3.1. Magnetization

The temperature dependences of *dc* magnetic susceptibility χ of $ACuFe_2(VO_4)_3$ are shown in Fig. 1. At elevated temperatures, $T \geq 150$ K, the curves can be fitted by a Curie – Weiss law

$$\chi = \chi_0 + C/(T-\Theta), \quad (1)$$

with similar sets of parameters, i.e., the temperature independent

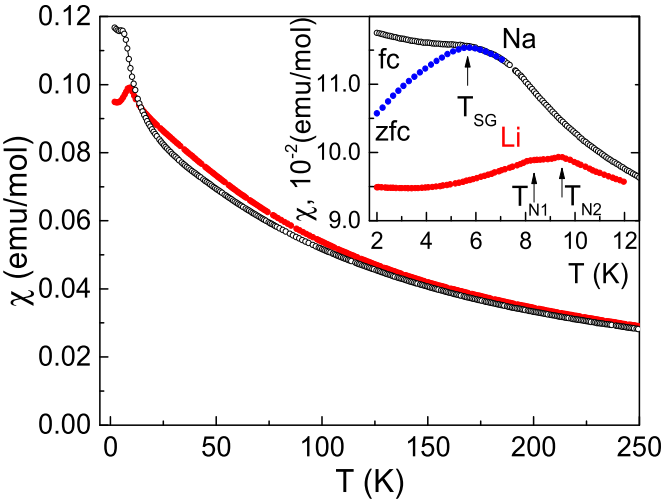

Fig. 1. Temperature dependences of magnetic susceptibility χ in $ACuFe_2(VO_4)_3$ taken in the *fc* regime at $B = 0.1$ T. The inset enlarges the low temperature region. An additional $\chi(T)$ curve taken in the *zfc* regime is shown for $NaCuFe_2(VO_4)_3$.

term $\chi_0 \sim -(4 \pm 2) \times 10^{-4}$ emu/mol and Curie constant $C = 9.2 \pm 0.2$ K emu/mol. The Weiss temperature $\Theta = -80 \pm 3$ K by far exceeds the magnetic ordering temperature $T_{N1} = 9.8$ K in $LiCuFe_2(VO_4)_3$. The temperature independent term is due to diamagnetic Pascal and Van Vleck contributions [9]. The Curie constant is defined by numbers of magnetic ions n_i, *g*-factors g_i and spins S_i of Cu^{2+} ($g > 2$, $S = 1/2$) and Fe^{3+} ($g = 2$, $S = 5/2$) ions according to summation $\Sigma n_i g_i^2 S_i(S_i+1) = 8C$. Negative Weiss temperatures indicate the predominance of antiferromagnetic exchange interactions in both Li and Na compounds at elevated temperatures. At low temperature, the $\chi(T)$ curves in the Na compound taken in field-cooled (*fc*) and zero-field-cooled (*zfc*) regimes spread, as shown in the inset to Fig. 1. Thus, the χ(T) data for Na compound hint on a spin-glass-like behavior at $T_{SG} \sim 6$ K which however do not exclude a disorder-broadened transition to the spin-ordered state. The Li compound evidences broad hump at about 30 K and two small peaks at $T_{N2} = 9.8$ K and $T_{N1} = 8.2$ K.

3.2. Specific heat

The temperature dependences of specific heat $C_p(T)$ in $ACuFe_2(VO_4)_3$ are shown in Fig. 2. At elevated temperatures, the specific heat of the Na compound exceeds that of the Li compound due to a

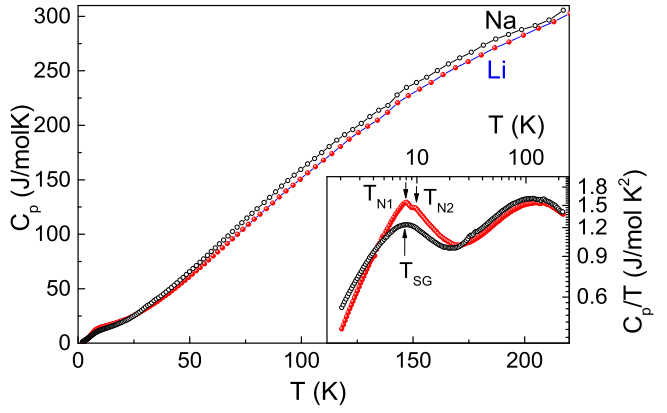

Fig. 2. The temperature dependences of specific heat in $ACuFe_2V_3O_{12}$. The inset represents the low temperature region in a double logarithm scale.

lower Debye temperature for A = Na. At low temperatures, the $C_p(T)$ curves evidence a double peak structure at T_{N2} = 9.8 K and T_{N1} = 8.2 K in $LiCuFe_2(VO_4)_3$ and a broad hump at T_{SG} ~ 8 K in $NaCuFe_2(VO_4)_3$. These features are shown in double logarithmic scale in the inset to Fig. 2. The data hence corroborate the findings of long-range magnetic order in $LiCuFe_2(VO_4)_3$ and a presumably glassy disordered phase in $NaCuFe_2(VO_4)_3$.

3.3. Permittivity

Fig. 3 shows the temperature dependences of the permittivity ε for $NaCuFe_2(VO_4)_3$, and its real ε′ and imaginary ε″ parts for $LiCuFe_2(VO_4)_3$. The Na compound demonstrates smoothly decreasing permittivity ε below room temperature, as shown in the upper panel of Fig. 3. In contrast, the Li compound shows non-monotonous behavior in both real ε′ and imaginary ε″ components, as shown in lower panel of Fig. 3. Sharp peaks denote the upper magnetic phase transition at T_{N2} = 9.8 K. The frequency dependent broad anomaly takes place at about 30 K. It has been shown in Ref. [3] that the sharp peak at T_{N2} is readily suppressed by external magnetic field which signifies a magnetoelectric effect, inherent for type II multiferroics. The frequency dependent feature at about 30 K follows an Arrhenius plot implying the relaxation process in the Li compound.

4. Resonant properties

4.1. Nuclear magnetic resonance

^{7}Li NMR ($I = 3/2$) spectra in $LiCuFe_2V_3O_{12}$ and ^{23}Na NMR ($I = 3/2$) spectra in $NaCuFe_2(VO_4)_3$ at various temperatures are shown in Fig. 4, left and middle panels, respectively. As temperature decreases from 300 K to 4 K, the spectra shift to higher frequency for both Li and Na compounds. The NMR shift is associated with the contact/transferred hyperfine coupling between the probing nuclei ^{7}Li and ^{23}Na and the magnetic moments of Cu^{2+} and Fe^{3+} in the host material due to hybridization of their wave functions. A nearly temperature independent NMR shift is due to the weakness of hyperfine coupling in the entire temperature range. The NMR spectra are narrow at high temperatures, but broaden gradually as temperature decreases which is attributed to the presence of many inequivalent static and slowly fluctuating hyperfine fields at ^{7}Li and ^{23}Na nuclear sites.

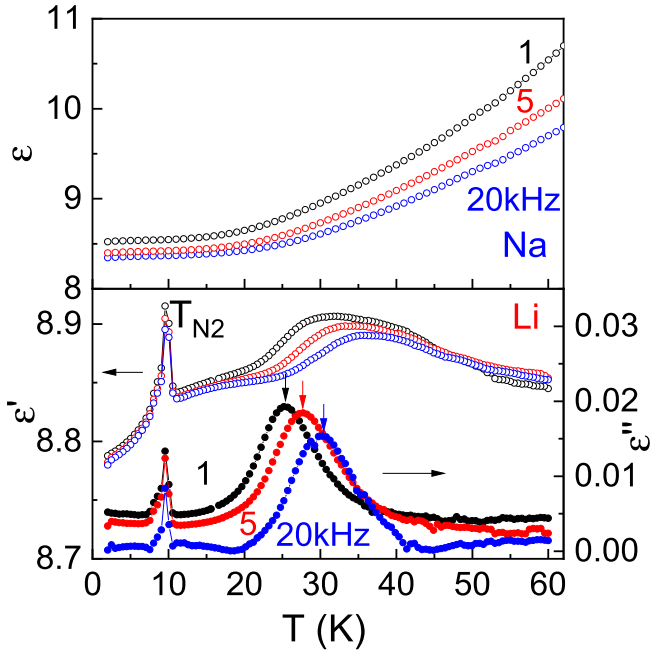

Fig. 3. The temperature dependences of dielectric permittivity ε in $NaCuFe_2(VO_4)_3$(upper panel) and its real ε′ and imaginary ε″ components in $LiCuFe_2(VO_4)_3$ (lower panel) taken at various frequencies.

As shown in the right panel of Fig. 4, the full width at half maximum (FWHM) of ^{7}Li and ^{23}Na NMR spectra progressively increases upon decreasing temperature and it is proportional to the bulk magnetic susceptibility χ measured at 0.1 T at high temperature ($20 \le T \le 225$ K) well above the magnetic ordering temperature. The broadening of ^{7}Li and ^{23}Na spectra is dominated by nuclear-nuclear dipolar and by hyperfine interaction of ^{7}Li and ^{23}Na nuclei with neighboring magnetic ions. In the Gaussian approximation [10,11] FWHM reads

$$FWHM \propto \sqrt{\langle \Delta\nu^2 \rangle_d + \langle \Delta\nu^2 \rangle_m}, \tag{2}$$

where $\langle \Delta\nu^2 \rangle_d$ is second moment of nuclear dipole-dipole interactions. In an external magnetic field B, anisotropic coupling gives rise to line broadening proportional to the static magnetic susceptibility, i.e.,

$$\frac{\sqrt{\langle \Delta\nu^2 \rangle_m}}{B} = A_z \chi, \tag{3}$$

where A_z is the average dipolar coupling constant between ^{7}Li or ^{23}Na nuclear moments and the neighboring magnetic moments. The fitting of FWHM vs. χ using Eq. (2) gives the value of dipolar coupling constant A_z between ^{7}Li/^{23}Na nuclei and Cu^{2+}/Fe^{3+} magnetic moments as $A_z = 1.0 \times 10^{22}$ cm^{-3} for both Li and Na compounds.

^{7}Li NMR and ^{23}Na spin lattice relaxation time measurements were carried out on both studied compounds to get insight into the spin correlations and spin dynamics in these materials. Generally, the nuclear spin lattice relaxation rate $1/T_1$ tracks the low energy spin fluctuations of electronic moments and is represented as the average of the imaginary part of dynamic electron spin susceptibility $\chi''(q,\omega)$ integrated over the wave vector q-space of the system under study [11,12];

$$\frac{1}{T_1 T} = \frac{2(\gamma_n)^2}{(g\mu_B)^2} k_B \sum_q \left| A_{hf} \right|^2 \frac{\chi''(q,\omega_n)}{\omega_n}, \tag{4}$$

where γ_n is gyromagnetic ratio, ω_n is the nuclear Larmor frequency, and A_{hf} is the q-dependent form factor of the hyperfine interactions between electronic moments. The ^{7}Li and ^{23}Na NMR spin-lattice relaxation rates ($1/T_1$) were measured at a field corresponding to the central peak position at each temperature in the temperature range $4 \le T \le 300$ K. In order to achieve better saturation, a train of 15–20 saturating pulses was applied. The recovery of the longitudinal magnetization is well described by a single exponential above 15 K. On the other hand, close to the ordering temperature, or below 15 K, the recoveries of both investigated compounds were best fitted with a stretched exponential function,

$$1 - \frac{M(t)}{M(0)} = A exp\left(- \left(\frac{t}{T_1} \right)^{\beta} \right). \tag{5}$$

The stretched exponential behavior of recovery of longitudinal magnetization below 15 K suggests inhomogeneous distribution of magnetic moments with inequivalent magnetic sites in the host lattice of both Na and Li compounds in the magnetically ordered state. The temperature dependence of the stretched exponent β is

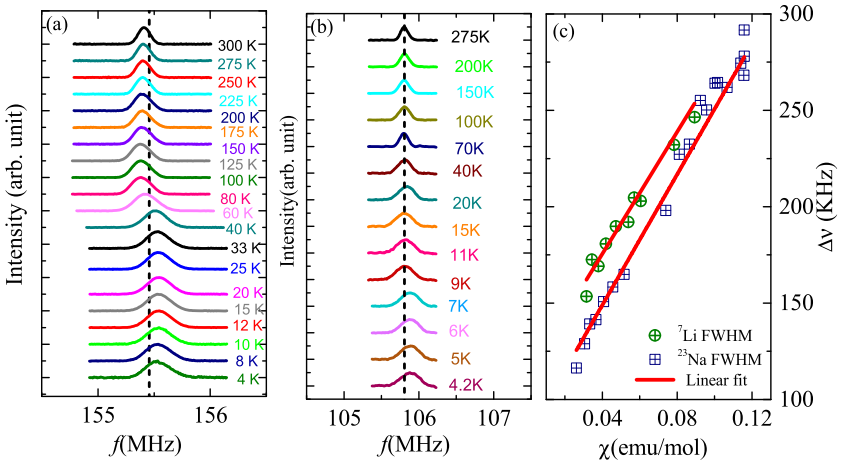

Fig. 4. ^{7}Li NMR (left panel) and ^{23}Na NMR spectra (middle panel) in $ACuFe_2(VO_4)_3$ (A = Li, Na) at various temperatures. The black dashed line represents the reference position of ^{7}Li and ^{23}Na nuclei at room temperature. The right panel shows the dependence of FWHM vs. bulk *dc* magnetic susceptibility measured at 0.1T field with temperature as an implicit parameter.

shown in the insets to Fig. 5.

As depicted in Fig. 5, the spin lattice relaxation rates $1/T_1$ above 20 K display *T*-independent behavior due to strong fluctuations of uncorrelated paramagnetic moments of Cu^{2+} and Fe^{3+} for both compounds. The gradual increase of spin lattice relaxations rates in the intermediate temperature range in both compounds suggests the presence of antiferromagnetic spin correlations consistent with magnetic susceptibility and NMR line width. In both compounds, the development of short-range spin correlations starts at temperatures comparable to the exchange couplings between magnetic moments inferring the presence of correlated spin dynamics before undergoing long range phase transitions in $LiCuFe_2(VO_4)_3$ and a spin-freezing state at low *T* in the case of $NaCuFe_2(VO_4)_3$. For $NaCuFe_2(VO_3)_4$, the appearance of maximum in $1/T_1$ close to T_{sg} is attributed to the fact that the frequencies of fluctuating but correlated magnetic moments, Cu^{2+} and Fe^{3+}, match with the Larmor frequencies of the respective probing ^{23}Na nuclei characteristic feature of disordered spin systems. This behavior of $1/T_1$ is consistent with the NMR line broadening at low *T*. The correlation frequency of magnetic moments is independent of temperature in the high *T* regime, while it depends on temperature in the low temperature limit [13–17].

The spin lattice relaxation rate, $1/T_1$, remains constant below the ordering temperature $T_{N1} = 8.2$ K in the Li compound, as also found in a handful of quantum magnets [18–20]. The origin of this unusual behavior of $1/T_1$ is not clear at present. We have plotted $1/\chi T_1 T$ as a function of temperature in the left panel of Fig. 6 for $LiCuFe_2(VO_4)_3$. $1/\chi T_1 T$ remains constant at high temperature and it increases below 50 K implying the development of short-range spin correlations in this temperature regime. It shows two transitions, one at $T_{N1} = 8.2$ K and another at 9.8 K confirming those found in bulk susceptibility and specific heat data. In the inset to left panel of Fig. 6 we show a few representative relaxation curves at selected temperatures. As shown in the right panel of Fig. 6, the intermediate and high *T* spin dynamics of the Na compound mimic those of the Li compound.

Fig. 7 shows the spin-spin relaxation rate $(1/T_2)$ as a function of temperature. It shows that the spin-spin correlation begins to increase below about 20 K and then leads to a prominent peak at $T_{N2} = 9.8$ K and a weak kink at $T_{N1} = 8.2$ K as in the case of $1/T_2$ in the Li compound. Below 15 K, we have fitted relaxation recovery of the transverse magnetization (Eq. (6))

$$\frac{M(t)}{M(0)} = A\exp\left(-\left(\frac{2t}{T_2}\right)^{\beta}\right) \tag{6}$$

for both systems by a single exponential ($\beta = 1$) to extract T_2, while Gaussian fits ($\beta = 2$) were carried out to extract T_2 at higher *T*.

As shown in Fig. 7, we found that $1/T_2$ is independent of temperature at high *T* for both compounds, which is associated with static contributions originated from nuclear dipolar interactions. The increase of $1/T_2$ in the intermediate regime is ascribed to hyperfine interaction between the probing nuclei and fluctuating magnetic moments. In $NaCuFe_2(VO_4)_3$, the enhancement of $1/T_1$ and $1/T_2$ suggests the slowing down of the spin dynamics on approaching the spin-freezing temperature, which is a typical

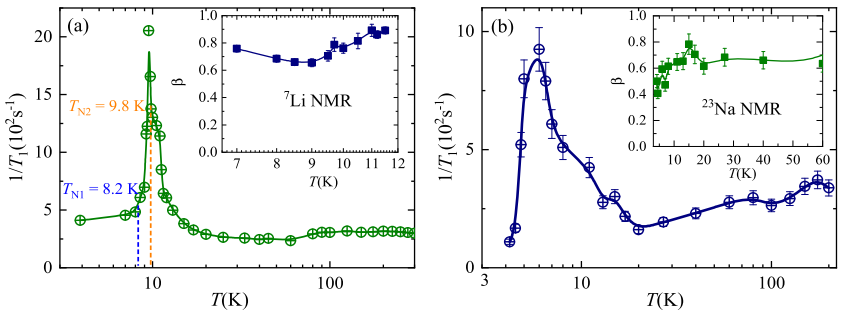

Fig. 5. Spin-lattice relaxation rate $(1/T_1)$ in $LiCuFe_2(VO_4)_3$ (a) and $NaCuFe_2(VO_4)_3$ (b) as a function of temperature. The insets show the *T*-variation of stretching exponent for both cases. Dashed vertical lines in (a) show anomaly temperatures as derived from bulk magnetization and specific heat data.

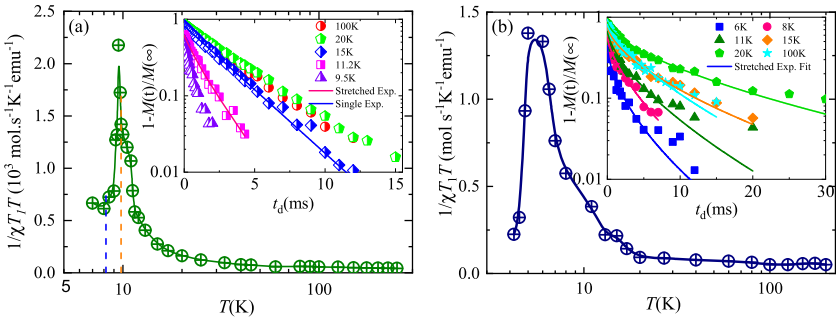

Fig. 6. Temperature dependence of the spin-lattice relaxation rate scaled with susceptibility and temperature ($1/\chi T_1 T$) for $LiCuFe_2(VO_4)_3$ (a) and $NaCuFe_2(VO_4)_3$ (b). The saturation recoveries of the longitudinal magnetization as a function of delay times at different temperatures are shown in the insets. The solid lines are the best fit for a single exponential (above 15 K) and a stretched exponential (below 15 K), respectively.

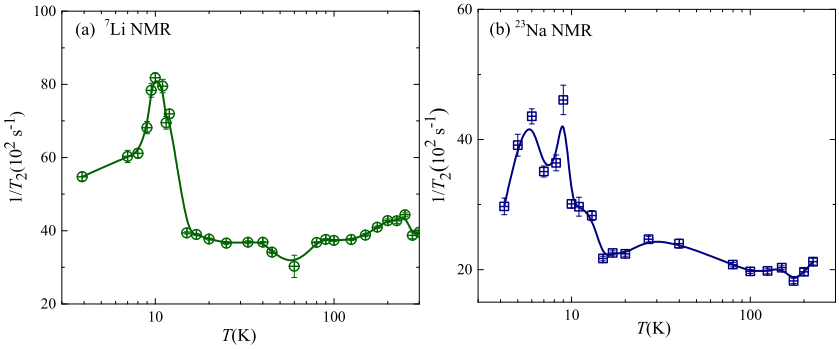

Fig. 7. The temperature dependence of the spin-spin relaxation rate ($1/T_2$) in $LiCuFe_2(VO_4)_3$ (a) and $NaCuFe_2(VO_4)_3$ (b).

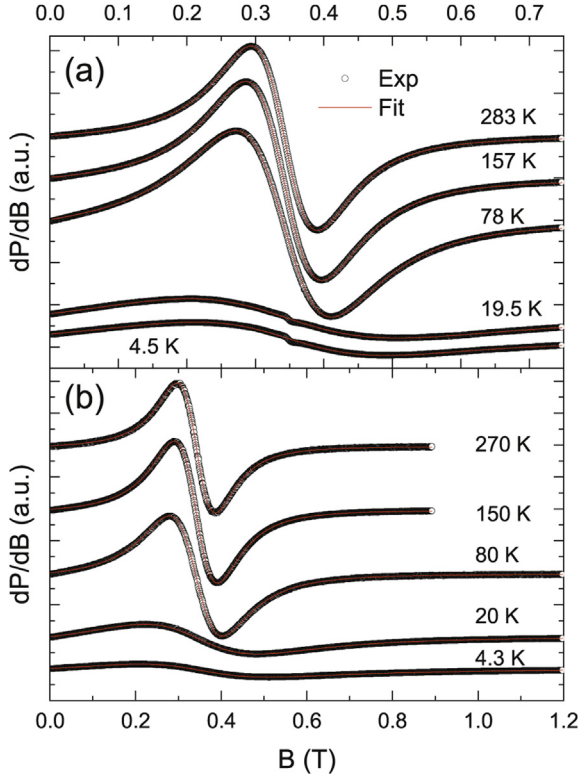

Fig. 8. X-ESR spectra of (a) $NaCuFe_2(VO_4)_3$ and (b) $LiCuFe_2(VO_4)_3$ at different temperatures. The symbols are experimental data and the red solid lines show fits as described in the text. (For interpretation of the references to color in this figure legend, the reader is referred to the Web version of this article.)

scenario in spin glass and disordered spin systems [17–21].

The symmetry breaking phase transition observed in local probe NMR measurements of the longitudinal relaxation rate (T_1^{-1}) and transverse relaxation rate (T_2^{-1}) are consistent with bulk magnetization and specific heat results. Inequivalent magnetic sites with competing energy scales in these systems lead to significant frustration manifested by short range spin correlations in a wide temperature range well above the transition temperature. Short range spin correlations are attributed to 26the presence of critical spin fluctuations mediated by frustration which is assumed to be the origin for non-trivial magnetic properties in these systems.

4.1.1. Electron spin resonance

X-Band ESR studies performed on $ACuFe_2(VO_4)_3$ evidence similar behavior in both systems. At high temperatures, there are quite broad resonance lines which, at 283 K (for A = Na) (270 K for A = Li), are well described by one Lorentzian with admixture of dispersion (mixing angle < 2°) and inclusion of a second order baseline, i.e.

$$\frac{dP}{dB} = -2I\frac{\Delta B(B-B_0)}{\left[(B-B_0)^2+\Delta B^2\right]^2} + \sin\left(\frac{\alpha\pi}{180}\right)\cdot I\frac{\Delta B^2-(B-B_0)^2}{\left[(B-B_0)^2+\Delta B^2\right]^2}, \quad (7)$$

where P is the power absorbed in the ESR measurement, I is the intensity of the measured signal, ΔB is the linewidth, B is the applied external static magnetic field, and B_0 is the resonance field.

Fitting of the data yields the effective g-factor g_{eff} = 2.010(6) (g_{eff} = 2.010(7)) and linewidth ΔB = 844(26) G (ΔB = 770(28) G) for Na and Li compounds, respectively. The observed g-factor can be attributed to the Fe^{3+} ions in an octahedral environment [22]. Note, that the

high-temperature spectra might be alternatively described by two Lorentzians, one of which being very weak. The *g*-factors of the additional, much weaker resonance amount to about 2.22 (for A = Na) and 2.36 (for A = Li). As *g*-factor anisotropy of this type is expected for Cu^{2+} in octahedral environment [23], the observed asymmetry of the resonance might be due to the anisotropic *g*-factor of Cu^{2+}. Considering the expected intensity of this resonance line, we however assess this scenario rather unlikely. This is in-line with a previous high-temperature ESR study on $LiCuFe_2(VO_4)_3$ which reports a single resonance [22]. In addition, the relevant ESR parameters of the main line are rather unaffected by the actual description of line shape down to about 100 K but fitting by two lines fails below that temperature. The fact that the high temperature ESR signal can be well described by a single Lorentzian implies that spin diffusion is not relevant in $ACuFe_2(VO_4)_3$ [24,25]. It also indicates strong isotropic exchange interaction being larger than the Zeeman energy [26].

Upon cooling down to about 30 K, the intensity of the ESR resonance increases monotonously. In particular, for both systems χ_{ESR} agrees very well with the static magnetic susceptibility, suggesting that the ESR and the static measurements are probing the same spins. In the low temperature region, the linewidth broadens critically which prevents the X-band measurement to capture the whole ESR signal and presumably causes the observed decrease of χ_{ESR} already above T_{N2}/T_{SG}. While B_{res} and hence g_{eff} hardly shift upon cooling down to about 30 K for A = Na and about 50 K for A = Li, there are pronounced changes of g_{eff} at lower temperature indicating the evolution of short-range antiferromagnetic correlations. The X-band ESR signals do not vanish upon evolution of long-range antiferromagnetic order and cooling down to 4.2 K which implies the presence of non-gapped magnon branches as, e.g., realized in easy plane-type antiferromagnets. As will be shown below, however, there are maxima of the linewidth in the vicinity of T_{N2}/T_{SG} and ΔB continuously decreases upon further cooling which may be associated with saturation of the spin correlation length and depletion of the spin fluctuation density due to depopulation of excited states, caused by the opening of a spin gap [27]. The obtained mixing angles (see Eq. (7)) are negligible for T > 30 K (40 K) for $NaCuFe_2(VO_4)_3$ ($LiCuFe_2(VO_4)_3$) and are explained by dispersion in the setup. Upon further cooling, however, it increases to 10°−20°. This must be attributed to changes in the dielectric constant which significantly affect the line shape of an ESR-resonance [28].

Upon cooling, the linewidth ΔB continuously increases which suggests critical behavior associated with the evolution of spin-spin correlations. Linewidth broadening can be described in terms of a power law of the reduced temperature, with the critical exponent *p* being associated with spin and spatial degrees of freedom. With the temperature independent linewidth ΔB_∞, the critical slowing down is analyzed as follows:

$$\Delta B(T) - \Delta B_\infty \propto \left(\frac{T - T_N}{T_N}\right)^{-p}. \quad (8)$$

Fits to the data according to Eq. (8) are shown in Fig. 9c and d (see Fig. 8). The data are well described down to about $3T_N$ below which non-linear behavior in the log-plot implies failure of a power law description. Using T_{SG} = 6.9 K and T_{N2} = 9.8 K for $NaCuFe_2(VO_4)_3$ and $LiCuFe_2(VO_4)_3$, respectively, we obtain p = 0.95(2) and ΔB_∞ = 72(2) mT (A = Na), and p = 0.72(2) and ΔB_∞ = 59(2) mT (A = Li).

Notably, despite clear differences in the low temperature behavior of the magnetic susceptibility, the specific heat, and the dielectric function, evolution of spin correlations towards the low temperature phase evolves very similar in both materials which is reflected by similar critical behavior. The obtained critical exponents are slightly smaller than those observed p = 1.2 ($CuCl2{\cdot}2NC5H5$) [29], p = 1.75 ($Bi_2Fe(SeO_3)_2OCl_3$) [30], p = 2.5 ($CsMnCl_3{\cdot}2H_2O$) [31]) for other quasi-one-dimensional spin systems. Exponents for two-dimensional spin systems are expected to be of similar magnitude while the presence of three-dimensional antiferromagnetic fluctuations is supposed to yield values of p = 0.66 (Heisenberg) and p = 0.59 (Ising) [32]. In low-dimensional systems, 3D-behaviour can establish, e.g., in crossover-type manner upon cooling towards T_N. Relatively small p even far above T_N are observed in systems with competing interactions. Thus, $p = 0.2 \div 0.9$ in a frustrated S = 1/2 square lattice ferromagnet [33], p = 0.47(2) in chiral $MnSb_2O_6$ [34], and $p \approx 0.50$ in a 2D quantum $SrCu_2(BO_3)_2$ [35] and Ising $MnTiO_3$ [36] antiferromagnets.

The fact that the ESR linewidth is described by Eq. (8), i.e., that it approaches a constant value at high temperatures, implies that the ESR signal is dominated by anisotropy effects while phonon-assisted spin-lattice broadening is negligible [37]. The continuous exponential growth of linewidth with decreasing temperature implies slowing down of spin fluctuations and the presence of strong short-range spin correlations at temperatures much larger than T_N [38]. The experimentally observed linewidths at high temperature and correspondingly the obtained values ΔB_∞ are comparable to what is found in exchange-coupled S = 5/2 spin systems with similar magnitude of magnetic interactions [30]. Quantitatively, ΔB_∞ is proportional to the ratio of the second moment M_2 of the resonance line and the exchange coupling according to [39].

$$\Delta B_\infty \approx \frac{20}{3\sqrt{3}} \frac{\hbar^2 M_2}{g\mu_B |J|}, \quad (9)$$

where g is the effective g - factor and J is the isotropic exchange coupling. The second moment may be, e.g., due to dipole-dipole, anisotropic, and Dzyaloshinskii-Moriya (DM) interactions. In fact, the latter can be excluded in the present case since the crystal structure of $ACuFe_2(VO_4)_3$ does not allow for the DM interactions. The second moment of the resonance line due to dipole-dipole interactions M_2^{DD} and anisotropic exchange interactions M_2^{AE}, given by [40].

$$M_2^{DD} = \frac{3g^4\mu_B^4}{\hbar^2}\left(\sum_{i>j}\frac{1}{r_{ij}^3}\right)^2 S(S+1), \quad \text{M} \quad (10)$$

$$M_2^{AE} = \frac{3}{\hbar^2}A^2 S(S+1), \quad (11)$$

can be used to estimate the temperature independent linewidth contribution. In Eqs. (10) and (11), r_{ij} is the distance between spins i and j, and A is the anisotropic exchange coupling, which is often estimated to be $|A| \approx (\Delta g\text{-}g)^2|J|$, with $\Delta g = g - 2$. The parameters used for an estimation of the linewidth are: S = 5/2 for Fe^{3+} ions, g = 2.01, r = 3.137 Å as the average distance between neighboring Fe^{3+} ions, and J = 1.24 meV as the average exchange coupling between neighboring Fe^{3+} as calculated below. With these parameters the linewidth contributions amount to $\Delta B_\infty^{DD} \approx$ 35 mT and $\Delta B_\infty^{AE} \approx 3 \times 10^{-4}$ mT. We hence attribute the broad line to dipolar contributions. Linewidth suggests short range order up to high temperature, i.e., large coupling. Thus, both systems exhibit similar critical behavior.

4.2. Mössbauer spectroscopy

Mössbauer spectra of $NaCuFe_2(VO_4)_3$ are shown in Fig. 10. The

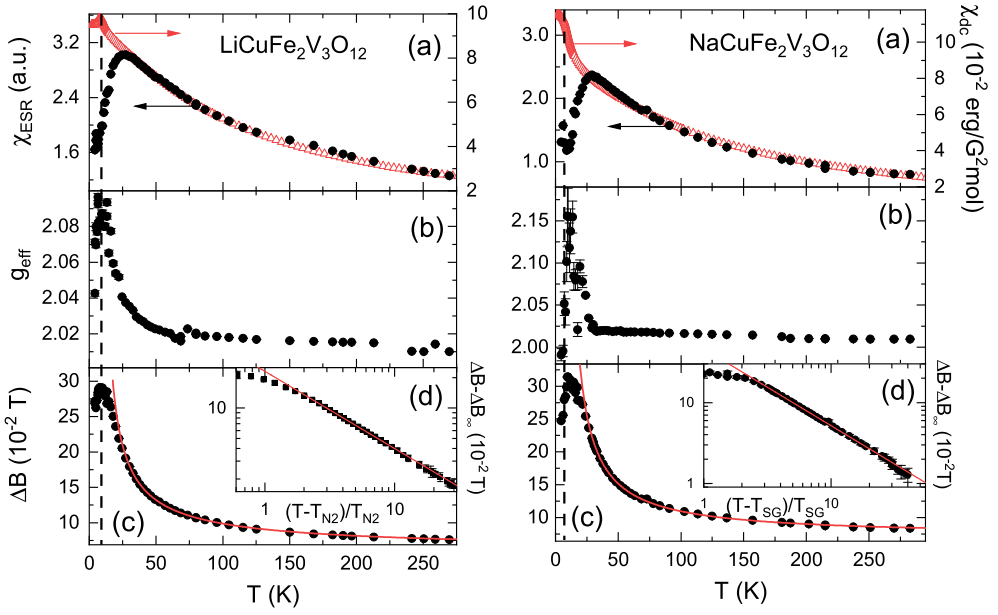

Fig. 9. Temperature dependence of (a) intensity of the ESR signal χ_{ESR}, (b) the effective g-factor g_{eff}, and (c) the linewidth ΔB in $LiCuFe_2(VO_4)_3$ (left panel) and $NaCuFe_2(VO_4)_3$ (right panel) obtained by lineshape fitting as described in the text. In (a) the static susceptibility χ from Fig. 1 is displayed, too. Black error bars are fit errors and gray error bars denote the difference to the results of fitting one Lorentzian without the admixture of dispersion. The vertical dashed line marks ordering and glass temperatures T_{N2} and T_{SG}, respectively. (d) shows a logarithmic plot of the linewidth and a fit to the data (see the text).

broad spectra require a complex fit model in the same way as it was in the case for $LiCuFe_2(VO_4)_3$. For comparison reason the analysis was done in a purely static picture similar to that given in Ref. [3]. The electric field gradient (EFG) was assumed axially symmetric with a principal component fixed to $V_{zz} = -43.5$ V/A^2 to fit the 15 K spectrum, which is slightly lower than for $LiCuFe_2(VO_4)_3$. The low temperature isomer shift with respect to room temperature iron $\delta(T \to 0) = 0.503(2)$ mm/s in the Na compound equals that in the Li compound. The model roughly fits the data and provides a temperature dependence of the parameters B_0 and σ shown in Fig. 11, which can be matched with the one of $LiCuFe_2(VO_4)_3$. The magnetic transition temperature is approximately 1 K lower in the case of $NaCuFe_2(VO_4)_3$, but there are no significant differences concerning the absolute values of the saturation hyperfine field $B_0(T \to 0)$ or the width σ.

5. First principles calculations

Here, we present the comparison of the first-principles studies on $NaCuFe_2(VO_4)_3$ with the similar studies on $LiCuFe_2(VO_4)_3$ [3].

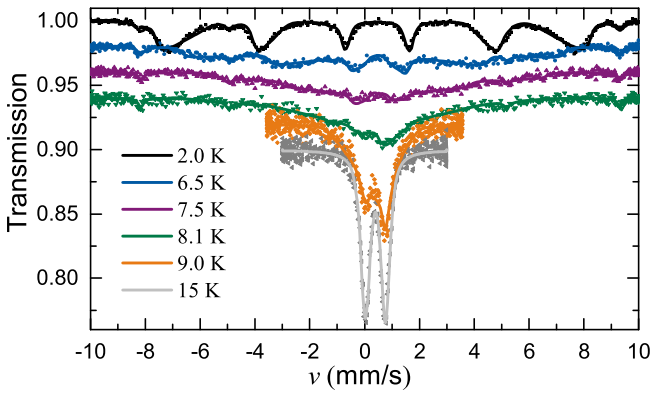

Fig. 10. $NaCuFe_2(VO_4)_3$ spectra fitted with static field distribution.

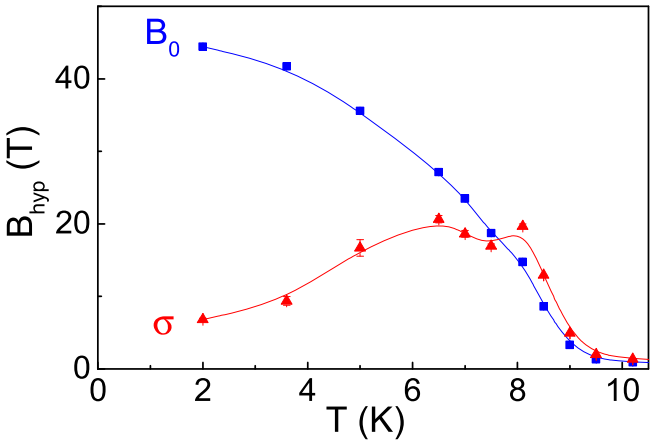

Fig. 11. The temperature dependences of the saturation hyperfine field B_0 and isomer shift σ in $NaCuFe_2(VO_4)_3$.

Towards this end, we first optimized the experimentally determined structure in a plane-wave basis [41] density functional theory (DFT) calculation with generalized gradient approximation (GGA) [42] for exchange-correlation functional by keeping lattice parameters and space group symmetry fixed. Only the positions of O atoms were relaxed toward equilibrium until the Hellman-Feynman force became less than 0.01 eV/Å during the optimization. All calculations were carried out on a theoretically optimized crystal structure.

The electronic density of states (DOS) for $NaCuFe_2(VO_4)_3$, obtained from non-spin polarized self-consistent calculation is presented in left panel of Fig. 12. The self-consistency was achieved by using an energy cutoff of 450 eV and $4 \times 2 \times 4$ Monkhorst-Pack k-points. We find the states close to Fermi level are mostly of Fe-d and Cu-d characters, with admixture of O-p character, which define the electronic and magnetic behavior of this compound. The spin-polarized DOS projected onto constituent atoms states is shown in

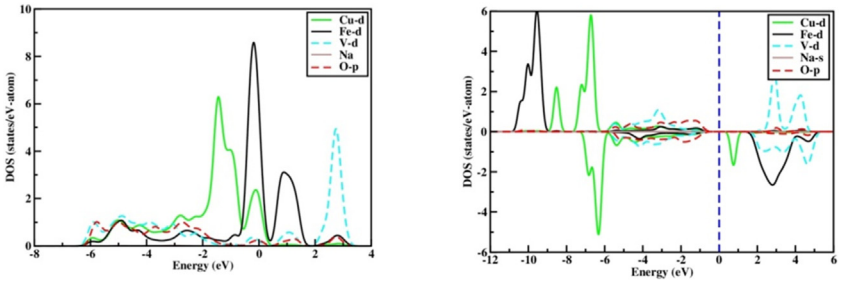

Fig. 12. Left panel: Electronic density of states (DOS) calculated using density functional theory of $NaCuFe_2(VO_4)_3$. The energy is plotted with respect to Fermi energy. Right panel: The spin polarized density of states of $NaCuFe_2(VO_4)_3$.

right panel of Fig. 12. The Fe-d states are filled in the majority spin channel and empty in the minority channel, meaning the 3+ valence of Fe while the Cu-d states are completely filled in both majority and minority channels except the minority channel of Cu-d_{x2-y2} meaning 2+ valence of Cu. The O-p state shows finite, non-zero hybridization with Fe-d and Cu-d states close to Fermi energy, which contributes to the super-exchange paths of magnetic interaction.

To calculate the leading magnetic couplings, we performed total energy calculation of different spin configurations of the magnetic ions in a 2x2x2 supercell. To account for the strong electron-electron correlation effect at Cu and Fe sites, calculations were carried within the GGA + U framework [43], with supplemented Hubbard U corrections at Cu and Fe sites. The Hubbard U value of late transition metal like Cu is expected to be larger than Fe. Following the estimates of constrained DFT calculations [44,45] we set the U values at Cu and Fe to be 8 eV and 4 eV, respectively with Hund's coupling J_H = 0.9 eV. We checked the influence of chosen U values by changing them by 1–2 eV. The trend of the results was found to remain unchanged. In particular, the magnetic moments differ by maximum 0.1 μ_B. The U values at Cu and Fe sites were chosen to be 8 eV and 4 eV, respectively with Hund's coupling J_H = 0.9 eV. The magnetic interactions between the magnetic ions are calculated by mapping the GGA + U energies to that of the Heisenberg model. The paths of leading magnetic interactions are shown in Fig. 13. The calculated values of magnetic exchanges for $NaCuFe_2(VO_4)_3$ are listed in Table 1 in comparison with that of $LiCuFe_2(VO_4)_3$. Obtained values are found to be close to that of $LiCuFe_2(VO_4)_3$ [3].

We also performed additional calculations including spin-orbit coupling considering collinear as well as non-collinear alignments of magnetic moments. Commencing with the collinear alignment of the spin and orbital moment having moments pointed along the *z* direction, relaxation within the non-collinear GGA + U + SOC calculations is found to produce nonzero components in the x and y directions (cf. Table 2) asserting the presence of finite spin-orbit coupling, especially at the Cu site. The value of the orbital magnetic moment at the Cu site is about 0.07 μ_B, which is non negligible. To derive the polarization through an inverse Dzyaloshinksii-Moriya interaction in the situation where the spatial symmetry gets broken in the magnetic structure, this large magnetic moment will take an important part. The moments of various ions as derived from GGA + U in the absence of any spin-orbit coupling are also listed in Table 2. The difference of the two also emphasizes the relative importance of the spin-orbit coupling.

Exchange interaction parameters in $NaCuFe_2(VO_4)_3$ similar to those calculated for $LiCuFe_2(VO_4)_3$ [1] were obtained for uniform distribution of the alkali ions within the channels of the howardevansite structure. There is, however, an important difference between these compounds with regards to the distribution of alkali ions in the half-filled positions. As shown in Fig. 14, the distance between two these positions in the Li compound amounts about 2.42 Å, which allows their simultaneous occupation and enables the correlated hopping process observed in experiment [7]. On the contrary, the distance between two half-occupied positions in the Na compound amounts to about 1.05 Å, which precludes their simultaneous occupation and restricts, in fact, cooperative hopping.

This fact leads, presumably, to uniform occupation of the half-filled positions within the channels in case of $LiCuFe_2(VO_4)_3$ and random occupation of these positions in case of $NaCuFe_2(VO_4)_3$, as

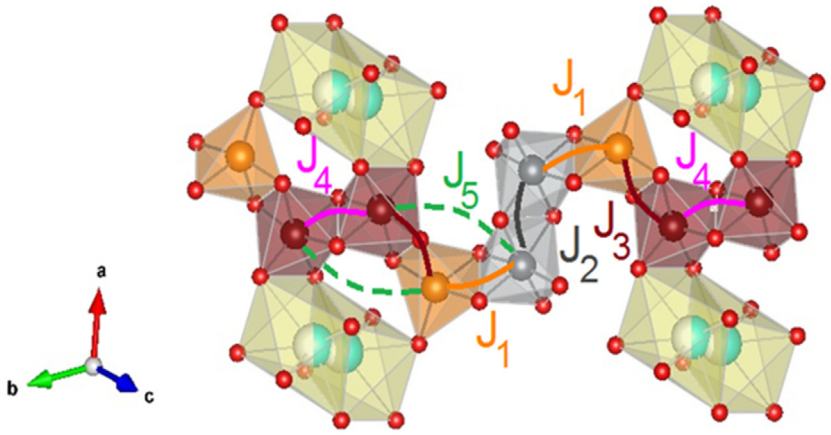

Fig. 13. Fragment of the crystal structure of $NaCuFe_2(VO_4)_3$ at room temperature. The solid and dashed arcs show NN and NNN magnetic exchange interactions within the chain. The orange, brown, gray, red and white-green colors represent Cu, Fe1, Fe2, O, and Na atoms, respectively. (For interpretation of the references to color in this figure legend, the reader is referred to the Web version of this article.)

Table 1
Magnetic exchange interaction parameters in $NaCuFe_2(VO_4)_3$ and $LiCuFe_2(VO_4)_3$. The positive (negative) signs of interactions indicate antiferromagnetic (ferromagnetic) nature of exchange interactions.

Interaction	Path	$NaCuFe_2(VO_4)_3$			$LiCuFe_2(VO_4)_3$ [1]		
		Bond angle	Bond-distance, Å	Value, meV	Bond angle	Bond-distance, Å	Value, meV
Nearest-neighbor intrachain	J1 Cu-O-Fe2	100.8°&98.8°	3.067	−0.16	99.9° &99.2°	3.074	−0.11
	J2 Fe2-O-Fe2	106.0°	3.185	1.24	104.2° &104.9°	3.112	1.02
	J3 Cu-O-Fe1	102.7°&100.2°	3.145	1.07	98.4° & 103.7°	3.121	1.08
	J4 Fe1-O-Fe1	103.0°	3.096	1.33	103.5° & 104.4°	3.156	1.38
Next-nearest-neighbor intrachain	J5 Cu-O-Fe1-O-F1	–	5.123	−0.11	–	5.122	−0.09
	J5′ Cu-O-Fe2-O-F2	–	5.176	−0.09	–	5.150	−0.01
	J5″ Fe1-O-Cu-O-Fe2	–	5.151	0.06	–	5.114	0.05
Interchain	J6 Fe1-O-V-O-Fe2	–	4.760	0.13	–	4.753	0.11

Table 2
Calculated magnetic moments (in μ_B) at different sites of $NaCuFe_2(VO_4)_3$ as obtained in GGA + U ($U_{Cu} = 8$ eV, $U_{Fe} = 4$ eV, $J_H = 0.8$ eV) and in GGA + U + SOC (shown in the parenthesis). For the GGA + U + SOC calculation, the spin and orbital moments in the x, y, and z directions are shown. For Na site, the magnetic moment is found to be vanishing in both calculations.

Cu	Fe	V	O	Na
0.70 (0.05, 0.05, 0.65; 0.02, 0.05, 0.07)	4.54 (0.08, 0.08, 4.53; 0.00, 0.00, 0.02)	0.14 (0.02, 0.01, 0.12; 0.00, 0.00, 0.01)	0.13 (0.01, 0.01, 0.12; 0.00, 0.00, 0.01)	0.00

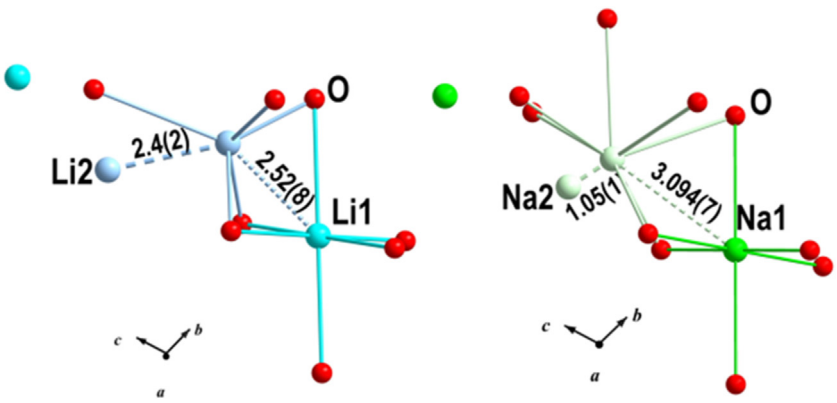

Fig. 14. Fragments of crystal structure of the Li and Na howardevansites showing positions of the alkali ions.

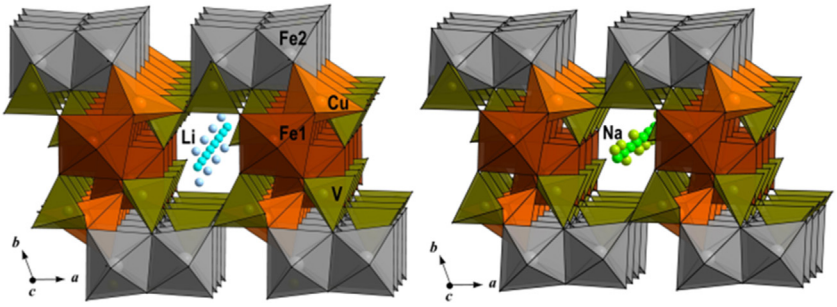

Fig. 15. The crystal structure of $LiCuFe_2(VO_4)_3$with uniform occupation of the half-filled positions of alkali ions and $NaCuFe_2(VO_4)_3$ with random occupation of these positions.

sketched in Fig. 15.

5.1. Conclusion

The pronounced differences in bulk properties of $LiCuFe_2(VO_4)_3$

and $NaCuFe_2(VO_4)_3$, i.e. magnetic susceptibility χ, specific heat C_p and electric permittivity ε, vanish at lowering the time scale of the microscopic resonant probe. We attribute this behavior to a different level of A-site disorder of the crystal structures as lower mobility of Na^+ ions within the channels of the howardevansite's structure [7] compared to the mobility of Li^+ ions [8] results in random freezing of the former ones. This randomness in $NaCuFe_2(VO_4)_3$ evidently perturbs a balance of exchange interactions necessary to stabilize the sequence of, presumably incommensurate and commensurate magnetic structures observed in $LiCuFe_2(VO_4)_3$at large length scales. Our local probe studies by means of nuclear magnetic resonance ($\tau \sim 10^{-9}$ s^{-1}), X-band electron spin resonance ($\tau \sim 10^{-11}$ s^{-1}) and Mössbauer spectroscopy ($\tau \sim 10^{-22}$ s^{-1}) provide information on the local magnetic properties at significantly smaller length scales. These compared to bulk methods instant snapshots reveal inherent similarity of both compounds supported by first principles calculations performed for a uniform distribution of alkali ions. Thus, another twist of multiferroicity of type II is found in the howardevansites, which is associated with the interplay of a fragile incommensurate/commensurate magnetic subsystem with the mobile electric subsystem of the alkali ions.

Declaration of competing interest

Authors confirm no conflict of interests.

CRediT authorship contribution statement

A. Koshelev: Conceptualization. **L. Shvanskaya:** Investigation. **O. Volkova:** Conceptualization. **K. Zakharov:** Investigation. **F. Theuss:** Investigation. **C. Koo:** Investigation. **R. Klingeler:** Supervision, Writing - original draft. **S. Kamusella:** Investigation. **H.-H. Klauss:** Supervision. **S. Kundu:** Investigation. **S. Bachhar:** Investigation. **A.V. Mahajan:** Supervision. **P. Khuntia:** Writing - original draft. **D. Khanam:** Investigation. **B. Rahaman:** Supervision. **T. Saha-Dasgupta:** Writing - original draft. **A. Vasiliev:** Conceptualization, Writing - review & editing.

Acknowledgements

This work has been supported by Russian Scientific Foundation through joint Russia — India Project No. 19-42-02010. PK acknowledges support from Department of Science and Technology, India through joint Indo-Russian project grant no. DST/INT/RUS/RSF/P-22. S. Kundu acknowledges financial support from IIT Madras. LS and AV acknowledge support by the Russian Ministry of Education and Science of the Russian Federation through NUST«-MISiS» Grant No. K2-2020- 008 and by the Act 211 of the Government of Russia, Contracts 02.A03.21.0004, 02.A03.21.0006 and 02.A03.21.0011. Support by Deutsche Forschungsgemeinschaft (DFG) via grant KL 1824/13-1 and Russian Foundation for Basic Research via grant 18-502-12022 is gratefully acknowledged.

References

[1] D. Khomskii, Different ways to combine magnetism and ferroelectricity, J. Magn. Magn Mater. 306 (2006) 1–8.
[2] M. Fiebig, T. Lottermoser, D. Meier, M. Trassin, The evolution of multiferroics, Nature Rev. Mater. 1 (2016) 16046.
[3] A.V. Koshelev, K.V. Zakharov, L.V. Shvanskaya, A.A. Shakin, D.A. Chareev, S. Kamusella, H.-H. Klauss, K. Molla, B. Rahaman, T. Saha-Dasgupta, A.P. Pyatakov, O.S. Volkova, A.N. Vasiliev, Spin-order-induced ferroelectricity and magnetoelectric effect in $LiCuFe_2(VO_4)_3$, Phys. Rev. Appl. 10 (2018), 034008.
[4] E. Vavilova, A.S. Moskvin, Y.C. Arango, A. Sotnikov, S.-L. Drechsler, R. Klingeler, O. Volkova, A. Vasiliev, V. Kataev, B. Buchner, Quantum electric dipole glass and frustrated magnetism near a critical point in Li_2ZrCuO_4, Eur. Phys. Lett. 88 (2009) 27001.
[5] J.M. Hughes, J.W. Drexler, C.F. Campana, M.L. Malinconico, Howardevansite, $NaCu^{2+}Fe^{3+}{}_2(VO_4)^{3-}{}_3$, a new fumarolic sublimate from Izalco Volcano, El Salvador; descriptive mineralogy and crystal structure, Am. Mineral. 73 (1988) 181–186.
[6] A.A. Belik, Synthesis and crystal structure of $LiCuFe_2(VO_4)_3$ by Rietveld method, Mater. Res. Bull. 34 (1999) 1973–1980.
[7] S. Kamoun, M. Gargouri, Electrical conductivity and complex electric modulus of $NaCuFe_2(VO_4)_3$ material, Ionics 21 (2015) 765–774.
[8] S. Kamoun, F. Hlel, M. Gargouri, Electrical properties and conductivity mechanism of $LiCuFe_2(VO_4)_3$, Ionics 20 (2014) 1103–1110.
[9] G.A. Bain, J.F. Berry, Diamagnetic corrections and Pascal's constants, J. Chem. Educ. 85 (2008) 532–536.
[10] P. Khuntia, M. Mariani, M.C. Mozzati, L. Sorace, F. Orsini, A. Lascialfari, F. Borsa, C. Maxim, M. Andruh, Magnetic properties and spin dynamics in the single-molecule paramagnets Cu_6Fe and Cu_6Co, Phys. Rev. B 80 (2009), 094413.
[11] C.P. Slichter, Principles of Magnetic Resonance, third ed., Springer, Berlin, 1996.
[12] A. Abragam, The Principles of Nuclear Magnetism, Clarendon, Oxford, U.K., 1960.
[13] D. Beeman, P. Pincus, Nuclear spin-lattice relaxation in magnetic insulators, Phys. Rev. 166 (1968) 359–375.
[14] M. Belesi, F. Borsa, A.K. Powell, Evidence for spin-wave excitations in the long-range magnetically ordered state of a Fe_{19} molecular crystal from proton NMR, Phys. Rev. B 74 (2006) 184408.
[15] R.J. Mahler, A.C. Daniel, P.T. Parrish, Observation of two intrinsic nuclear relaxation rates in antiferromagnetic $KMnF_3$, Phys. Rev. Lett. 19 (1967) 85–87.
[16] W.-J. Lee, S.-H. Do, S. Yoon, Z.H. Jang, B.J. Suh, J.H. Lee, A.P. Reyes, P.L. Kuhns, H. Luetkens, K.-Y. Choi, Anomalous spin dynamics in $CdCu_2(BO_3)_2$ revealed by ^{11}B NMR and ZF-μSR, Phys. Rev. B 90 (2014) 214416.
[17] P. Khuntia, F. Bert, P. Mendels, B. Koteswararao, A.V. Mahajan, M. Baenitz, F.C. Chou, C. Baines, A. Amato, Y. Furukawa, Spin liquid state in the 3D frustrated antiferromagnet $PbCuTe_2O_6$: NMR and muon spin relaxation studies, Phys. Rev. Lett. 116 (2016) 107203.
[18] A.W. Hunt, P.M. Singer, K.R. Thurber, T. Imai, 63Cu NQR measurement of stripe order parameter in $La_{2-x}Sr_xCuO_4$, Phys. Rev. Lett. 82 (1999) 4300–4303.
[19] D.A. Levitt, R.E. Walsted, Comments on "Host nuclear resonance in a spin-glass: CuMn, Phys. Rev. Lett. 38 (1977) 178–181.
[20] A. Olariu, P. Mendels, F. Bert, B.G. Ueland, P. Schiffer, R.F. Berger, R.J. Cava, Unconventional dynamics in triangular heisenberg antiferromagnet $NaCrO_2$, Phys. Rev. Lett. 97 (2006) 167203.
[21] N. Bloembergen, E.M. Purcell, R.V. Pound, Relaxation effects in nuclear magnetic resonance absorption, Phys. Rev. 73 (1948) 679–712.
[22] T. Drokina, G. Petrakovskii, O. Bayukov, A. Vorotynov, D. Velikanov, M. Molokeev, Synthesis and structural, magnetic, and resonance properties of the $LiCuFe_2(VO_4)_3$ compound, Phys. Solid State 58 (2016) 1981–1988.
[23] C. Koo, E.A. Zvereva, I.L. Shukaev, M. Richter, M.I. Stratan, A.N. Vasiliev, V.B. Nalbandyan, R. Klingeler, Static and dynamic magnetic response of fragmented haldane-like spin chains in layered $Li_3Cu_2SbO_6$, J. Phys. Soc. Jpn. 85 (2016), 084702.
[24] R. Dietz, F. Merritt, R. Dingle, D. Hone, B. Silbernagel, P.M. Richards, Exchange narrowing in one-dimensional systems, Phys. Rev. Lett. 26 (1971) 1186.
[25] M.J. Hennessy, C.D. McElwee, P.M. Richards, Effect of interchain coupling on electron-spin resonance in nearly one-dimensional systems, Phys. Rev. B 7 (1973) 930–947.
[26] M. Oshikawa, I. Affleck, Electron spin resonance in =1/2 antiferromagnetic chains, Phys. Rev. B 65 (2002) 134410.
[27] F. Chabre, A. Ghorayeb, P. Millet, V. Pashchenko, A. Stepanov, Low-temperature behavior of the ESR linewidth in a system with a spin gap: η-$Na_{1.286}V_2O_5$, Phys. Rev. B 72 (2005), 012415.
[28] M. Sueki, G.A. Rinard, S.S. Eaton, G.R. Eaton, Impact of high-dielectric-loss materials on the MicrowaveField in EPR experiments, J. Magn. Reson. A 118 (1996) 173–188.
[29] Y. Ajiro, S. Matsukawa, T. Yamada, T. Haseda, Temperature dependence of the ESR line width in one-dimensional S=1/2 antiferromagnet $CuCl_2{\cdot}2NC_5H_5$, J. Phys. Soc. Jpn. 39 (1975) 259–260.
[30] P.S. Berdonosov, E.S. Kuznetsova, V.A. Dolgikh, A.V. Sobolev, I.A. Presniakov, A.V. Olenev, B. Rahaman, T. Saha-Dasgupta, K.V. Zakharov, E.A. Zvereva, O.S. Volkova, A.N. Vasiliev, Crystal structure, physical properties, and electronic and magnetic structure of the spin S = 5/2 zigzag chain compound $Bi_2Fe(SeO_3)_2OCl_3$, Inorg. Chem. 53 (2014) 5830–5838.
[31] Y. Tazuke, K. Nagata, EPR line-widths of a one-dimensional heisenberg antiferromagnet $CsMnCl_32H_2O$, J. Phys. Soc. Jpn. 38 (1975) 1003–1010.
[32] H. Benner, J.P. Boucher, in: L.J. De Jongh (Ed.), Magnetic Properties of Layered Transition Metal Compounds, Kluwer, Dordrecht, 1990.
[33] T. Förster, F. Garcia, T. Gruner, E.E. Kaul, B. Schmidt, C. Geibel, J. Sichelschmidt, Spin fluctuations with two-dimensional XY behavior in a frustrated S=1/2 square-lattice ferromagnet, Phys. Rev. B 87 (2013) 180401.
[34] J. Werner, C. Koo, R. Klingeler, A. Vasiliev, Y. Ovchenkov, A. Polovkova, G. Raganyan, E. Zvereva, Magnetic anisotropy and the phase diagram of chiral $MnSb_2O_6$, Phys. Rev. B 94 (2016) 104408.
[35] A. Zorko, D. Arcon, A. Lappas, J. Giapintzakis, Near critical behavior in the two-dimensional spin-gap system $SrCu_2(BO_3)_2$, Phys. Rev. B 65 (2001), 024417.
[36] J. Akimitsu, Y. Ishikawa, Magnetic critical behavior of a quasi two-dimensional

antiferromagnet $MnTiO_3$, J. Phys. Soc. Jpn. 42 (1977) 462–469.
[37] D.L. Huber, Exchange narrowing of the phonon contribution to the electron spin resonance line width in exchange-coupled magnetic insulators, J. Phys. Condens. Matter 26 (2014), 056002.
[38] A.G. Anders, S.V. Volotski, EPR in 1-d and 2-d antiferromagnetic systems, J. Magn. Magn Mater. 31 (1983) 1169–1170.
[39] R. Kubo, K. Tomita, A general theory of magnetic resonance absorption, J. Phys. Soc. Jpn. 9 (1954) 888–919.
[40] I. Yamada, M. Nishi, J. Akimitsu, Electron paramagnetic resonance governed by the Dzyaloshinsky–Moriya antisymmetric exchange interaction in $CuGeO_3$, J. Phys. Condens. Matter 8 (1996) 2625–2640.
[41] W. Kohn, L.J. Sham, Self-consistent equations including exchange and correlation effects, Phys. Rev. A 140 (1965) 1133–1138.
[42] J.P. Perdew, K. Burke, M. Ernzerhof, Generalized gradient approximation made simple, Phys. Rev. Lett. 77 (1996) 3865–3868.
[43] V.I. Anisimov, I.V. Solovyov, M.A. Korotin, M.T. Czyzyk, G.A. Sawatzky, Density-functional theory and NiO photoemission spectra, Phys. Rev. B 48 (1993) 16929.
[44] A.K. McMahan, R.M. Martin, S. Satpathy, Calculated effective Hamiltonian for La_2CuO_4 and solution in the impurity Anderson approximation, Phys. Rev. B 38 (1988) 6650.
[45] Z. Zhang, S. Satpathy, Electron states, magnetism, and the Verwey transition in magnetite, Phys. Rev. B 44 (1991) 13319.